Available online at www.sciencedirect.com
ScienceDirect
Acta Biomaterialia 5 (2009) 2084–2094
Acta BIOMATERIALIA
www.elsevier.com/locate/actabiomat

Effects of filler type and content on mechanical properties of photopolymerizable composites measured across two-dimensional combinatorial arrays

Sheng Lin-Gibson [a,*], Lipiin Sung [b], Aaron M. Forster [b], Haiqing Hu [b], Yajun Cheng [a], Nancy J. Lin [a]

[a] Polymers Division, National Institute of Standards and Technology, Gaithersburg, MD 20899-8543, USA
[b] Materials and Construction Research Division, National Institute of Standards and Technology, Gaithersburg, MD 20899-8615, USA

Received 21 July 2008; received in revised form 12 December 2008; accepted 26 January 2009
Available online 5 February 2009

Abstract

Multicomponent formulations coupled with complex processing conditions govern the final properties of photopolymerizable dental composites. In this study, a single test substrate was fabricated to support multiple formulations with a gradient in degree of conversion (DC), allowing the evaluation of multiple processing conditions and formulations on one specimen. Mechanical properties and damage response were evaluated as a function of filler type/content and irradiation. DC, surface roughness, modulus, hardness, scratch deformation and cytotoxicity were quantified using techniques including near-infrared spectroscopy, laser confocal scanning microscopy, depth-sensing indentation, scratch testing and cell viability. Scratch parameters (depth, width, percent recovery) were correlated to composite modulus and hardness. Total filler content, nanofiller and irradiation time/intensity all affected the final properties, with the dominant factor for improved properties being a higher DC. This combinatorial platform accelerates the screening of dental composites through the direct comparison of properties and processing conditions across the same sample.
Published by Elsevier Ltd. on behalf of Acta Materialia Inc.

Keywords: Combinatorial; Composite; Cytotoxicity; Nanoindentation; Scratch test

1. Introduction

Dental composites are complex systems comprising a photopolymerizable binary or ternary resin mixture filled with inorganic particles. As such, a large number of chemical and processing parameters influence their properties [1]. For a given resin system, the size and concentration (loading) of the fillers used to reinforce the composite affect the final properties. The filler concentration is often dictated by the target application. For example, flowable dental adhesives are lightly filled, whereas composites for restoring posterior teeth are highly filled to withstand the greater forces of mastication. A high filler loading is advantageous because it leads to superior composite strength and reduced photopolymerization-induced shrinkage. The size of the filler particles also affects the composite properties. For instance, commercial dental composites are often filled with both micron-size and nano-size particles. Micron-size particles are used to increase filler content while retaining processability, while nanofillers are incorporated to increase wear resistance [1].

Dental composites must meet a stringent series of performance benchmarks to achieve clinical acceptance. Because of the complexity in the composite formulation, systematic variation of formulation parameters and subsequent screening of multiple properties on a large number of samples is time consuming, laborious and often impractical. In the most complete studies involving reaction kinetics, conversion, physical/mechanical properties and

* Corresponding author. Tel.: +1 301 975 6765; fax: +1 301 975 4977.
E-mail address: slgibson@nist.gov (S. Lin-Gibson).

1742-7061/$ - see front matter Published by Elsevier Ltd. on behalf of Acta Materialia Inc.
doi:10.1016/j.actbio.2009.01.043

biocompatibility, only a single formulation is considered. Yet material and processing parameters are intertwined such that one formulation may exhibit weak performance improvements, while a slightly different formulation exhibits significant performance improvements. This complexity underscores the importance of screening a large number of parameters, as a single formulation that optimizes all properties often does not exist.

High-throughput and combinatorial (HT&C) methods using either continuous gradient or discrete array libraries have the advantages of faster data acquisition, wider examination of experimental variables, equal processing conditions for a given specimen, and greater experimental statistics over traditional one-at-a-time methods [2]. Material properties can be characterized and analyzed over a large parameter space by fabricating an array specimen varying in two material parameters. In addition, multiple chemical and physical characterization techniques may be employed on the same specimen to allow a thorough structure–property characterization. The ability to compare multiple properties on the same platform is especially suitable for photopolymerized dimethacrylate polymers, because the resulting material properties vary greatly depending on the sample preparation procedure. Preparing a series of systematically varied, individual samples for multiple material property characterization is a challenging task given the sensitivity of the photopolymerization process to changes in light intensity and sample geometry; thus, combinatorial approaches are advantageous for these materials.

Various fabrication and characterization tools for rapid measurement and analysis have been adapted for HT&C methods. Spectroscopy such as Fourier transform infrared (FTIR) spectroscopy, FTIR in reflectance mode (RM) [3], near-infrared (NIR) spectroscopy [4] and Raman [5] are ideal for determining chemical information. The surface morphology can be characterized by microscopy techniques including optical and confocal microscopy. In addition, depth-sensing indentation (DSI) testing or nanoindentation is well suited for mechanical property measurements [4,6–8] and has been demonstrated to be useful in the characterization of dental composites, ceramics and alloys [9,10]. Recently, the indenter probe has been used to produce well-controlled scratches with either a constant load or progressively increasing load (progressive-load scratch) with the resultant scratches characterized by confocal microscopy or light scattering [11,12]. The scratch resistance and polymer relaxations (elastic–plastic transition and scratch damage patterns) can provide additional insight into time- or strain-dependent material properties. For materials used in biomedical applications such as dental restorations, biocompatibility is another critical concern. HT&C methods have been shown to increase the throughput of bioassays [13] when characterizing biocompatibility of materials.

We have been utilizing HT&C methods to screen multiple properties of dental polymers. Our previous studies focused on two-dimensional (2-D) composition arrays and degree of conversion (DC) gradients of dental polymers using a monomer system consisting of binary mixtures of bisphenol A-glycidyl dimethacrylate (BisGMA) and triethylene glycol dimethacrylate (TEGDMA) [14]. We have also studied biocompatibilities of dental polymers [13,14] and composites [15] using 2-D platforms. In the current study, we investigated the effects of filler size and concentration on various chemical, physical and mechanical properties, in addition to biological properties. Cell studies were performed using a macrophage cell line, as macrophages are mediators of the inflammatory reaction and have been shown to be useful when evaluating the cellular responses to dental materials [16–18]. All measurements were performed on the same samples – the 2-D specimens – thus allowing direct comparison of the data. A suite of methods that includes NIR spectroscopy, laser scanning confocal microscopy (LSCM), DSI testing, scratch tests coupled to imaging, and bioassays modified specifically for combinatorial studies provide insight into the effects of composition/irradiation on properties. All of the properties examined have a critical impact on the clinical performance of dental composites.

2. Materials and methods

2.1. Materials

Resins BisGMA and TEGDMA were obtained from Esstech Inc. Photoinitiator system components, camphorquinone (CQ) and ethyl 4-*N*,*N*-dimethylaminobenzoate (4E), were purchased from Aldrich Corp. The SP 345 silane glass filler (SG, 0.70 μm average diameter) and fumed amorphous silica filler (OX50, 0.04 μm average diameter) were provided by the L.D. Caulk Company. Methacryloxypropyltrimethoxysilane (MPTMS) and *n*-octadecyltrimethoxysilane (OTMS) were purchased from Gelest, Inc. Cell culture reagents were purchased from Invitrogen Corp., unless otherwise noted. All reagents were used as received.

2.2. Composite preparation

BisGMA and TEGDMA (mass ratio = 50:50) were activated for blue light photopolymerization with 0.2% CQ and 0.8% 4E (by mass) and stored in the dark until use. The SG and OX50 fillers were mixed into the activated resin following the formulations shown in Table 1. The 2-D specimens consisted of a discrete array in composite formulation (individual stripes) along one axis with an orthogonal gradient in methacrylate conversion.

The specimens were fabricated by adapting procedures previously used for specimens of unfilled polymers [14]. Briefly, a sample mold was prepared using two glass slides (50 mm × 75 mm), a polyester release film and a poly(dimethylsiloxane) spacer (thickness ≈1.5 mm) with five channels (3 mm × 60 mm). The spacer was placed on top of a glass slide covered with a release film, and then

Table 1
Composite formulations.

Formulation	Activated Resin (% by mass)	SG (% by mass)	OX50 (% by mass)
S1	35	65	0
S2	50	50	0
S3	50	45	5
S4	65	30	5
S5	80	15	5

the composite mixtures were spread into the distinct channels. The second glass slide, surface treated with MPTMS to enhance adhesion of the dimethacrylate polymer, was placed over the sample, and the entire assembly was clamped together. The conversion gradients were generated using the following polymerization protocol. First, the assembly was placed 10 cm beneath a light source (Dentsply Triad 2000 replacement tungsten halogen light bulb, 120 V, 250 W). The irradiation intensity from this source decreases exponentially, with the highest irradiation occurring directly underneath the center of the light source [13]. The sample was positioned with one edge directly under the center of the light source and irradiated for 15 s per side. This process produced a DC gradient, but the DC range was relatively narrow with a maximum DC less than 60% [13], much lower than that possible. To increase the DC on the high conversion end, a shield was used to cover most of the sample, leaving approximately 10 mm of the high DC end exposed. The specimen was then further cured for 1 min per side. A schematic of the setup is provided in an earlier publication [14]. Specimens were stored in the dark for 24 h prior to characterization to ensure that the DC no longer changed with time. A notch was made across the DC gradient at the high conversion end and defined as the zero position for subsequent measurements.

2.3. NIR spectroscopy

Transmission NIR spectroscopy was performed using a Nicolet Magna 550 FTIR spectrometer (Madison, WI) configured with a white light source, a CaF_2 beam splitter and an InSb detector. The NIR spectra in the region of 7000–4000 cm^{-1} were acquired from 32 averaged scans at 6 cm^{-1} resolution. The NIR beam was placed at discrete locations along the gradient sample to measure DC. DC was quantified as 1 minus the ratio of the residual methacrylate C=C stretch (4743 cm^{-1}) peak height in the polymerized sample to the same peak in the uncured composite paste [4]. In addition, each peak was normalized to the aromatic peak height (4623 cm^{-1}) from the same sample. Conversion measurements were collected over 50 mm at 10 mm intervals. The relative uncertainty associated with the NIR measurements is 3%.

2.4. LSCM for surface roughness characterization

Surface morphology and root-mean-square (RMS) surface roughness were measured by reflection LSCM (laser wavelength = 543 nm) [19,20]. A 10× and a 50× objective were used to scan an area of 921.4 μm × 921.4 μm and 184.3 μm × 184.3 μm, respectively. At each location, a 2-D intensity projection of the surface was prepared by summing the stack of images over the z-direction, 512 pixels × 512 pixels. A 2-D projection image is effectively the sum of the light back-scattered by different z-layers of the surface as far into the composite as possible. The pixel intensity level represents the total amount of back-scattered light, with lighter areas representing regions scattering more light.

2.5. Mechanical testing

DSI measurements were performed using a MTS Nanoinstruments NanoXP instrument (Oak Ridge, TN) equipped with a 10 μm radius, 90° diamond cone indenter. The contact stiffness between the sample and tip was measured by superposing a small oscillation (45 Hz, 5 nm) over the load profile. This contact stiffness was used to calculate the elastic modulus of the sample [21,22] using a constant Poisson's ratio of 0.45, a value found to be representative for dental composites [23]. The modulus and hardness were determined as the average value obtained over a depth ranging from 1000 to 4000 nm. The hardness to modulus ratio (H/E) was calculated from these averages. All indentation experiments were conducted using a constant indentation strain rate of 0.05 s^{-1}. Mechanical data were collected and reported over a 50 mm length at 10 mm intervals beginning at the zero position for each composition. Three indents ($n = 3$) were measured at each location. The standard uncertainty associated with the DSI measurements is 5%.

The surface of each composite was scratched parallel to the conversion gradient ($n = 3$) and within 1 mm of each indent location using the same indenter (10 μm radius, 90° diamond cone tip). A progressive-load scratch method was used to produce three 400 μm scratches parallel to the curing gradient from 0 to 50 mm at 10 mm intervals. The test involved three distinct steps. First, a surface profile was collected using the indenter tip at a contact force of 20 μN. Then, the progressive-load scratch (initial penetration) was performed at a scratch velocity of 10 μm s^{-1} with a linear normal force increase from nominally 20 μN to approximately 50 mN. Finally, a post-scratch profile (residual penetration) was generated at a 20 μN contact force to quantify plastic deformation. All profiles were taken within 10 min of each other. To evaluate the mode of deformation and the scratch recovery, initial penetration depth (d_i), residual penetration depth (d_r) and percent recovery ($(d_i - d_r)/d_i$) were calculated. LSCM (150× objective) was used to characterize the scratch morphology, including scratch width (W_p), full depth (D_f) and the scratch damage patterns [24]. The scratch width (W_p) was defined as the peak-to-peak distance perpendicular to the scratch length. The W_p/D_f ratio was also calculated. The standard uncertainty associated with the scratch measurements is 5%.

For comparison, composite moduli were also measured using a universal testing machine (model 5500R, Instron Corp., MA). Specimens with a width and height of approximately 2 mm and a uniformly high conversion were prepared using the same formulations as the testing platform (Table 1). A standard three-point flexural configuration with a span of 20 mm was used with a crosshead speed of 0.5 mm/min^{-1}.

2.6. Cell viability

Viability of macrophages on the samples was assessed as previously described [15]. Briefly, RAW 264.7 murine macrophage-like cells (American Type Culture Collection, ATCC TIB-71) were cultured in Roswell Park Memorial Institute (RPMI) 1640 growth medium containing 10% (by volume) heat-inactivated fetal bovine serum. Gradient substrates were sterilized using ethylene oxide gas and aged in phosphate-buffered saline (PBS) for 7 days. Cells were seeded directly onto the substrates and onto negative control tissue culture polystyrene plates for a final cell density of 2.5×10^4 cells cm^{-2}.

After culturing for 24 h in a humidified incubator (37 °C, 5% CO_2 by volume), cells were stained for viability using growth medium containing calcein acetoxymethyl ester (calcein AM, live cells, 2 μmol l^{-1}), ethidium homodimer-1 (EthD-1, dead cells, 2 μmol l^{-1}) and Hoechst 33342 (H33342, all cells, 10 μmol l^{-1}) [14] and imaged on a Leica DMA epifluorescence microscope.

3. Results and discussion

We have developed a method to screen multiple properties of photopolymerized composites over a large parameter space using a 2-D array. The composite samples varied in chemical composition (e.g. filler size/concentration) and DC on orthogonal axes (Fig. 1A). Chemical compositions (S1–S5, Table 1) were kept discrete and were based on the same resin system, while the filler size (macrofiller and/or nanofiller) and mass fraction were varied to investigate their effects on material properties. Each composition was then polymerized to form a gradient in DC (high DC end at 0 mm). As will be discussed, the array sample was successfully used to identify significant differences in surface roughness, reaction kinetics, mechanical properties and cell viability as a function of filler type/content and DC.

With the addition of fillers, the first noticeable effect in the composites was the morphology of the free (air–composite) surface. Unlike neat polymer gradients, where the surface remained smooth along the entire conversion gradient [13], composites cured with reduced irradiation time and intensity exhibited an increased surface roughness at lower DC. Projection views of the surface roughness, generated using confocal microscopy, revealed a generally smooth surface at high DC that became progressively rougher with decreasing DC (Fig. 1A). The same trend was observed for all compositions and using two different microscope objectives. The mechanism for generating the roughness gradient is likely associated with the photopolymerization protocol and is the subject of further investigation. Polymerization of dimethacrylates is known to be accompanied by a significant amount of shrinkage [25]. In the presence of non-shrinking fillers, the polymer may contract away from filler particles that have been immobilized upon vitrification, thus creating uneven shallow grooves and pits on the surface. This explanation is plausible since the polymerization shrinkage generally lags behind the gel point [26].

The RMS roughness values were calculated from 3-D confocal microscopy images for each composition as a function of position. As mentioned previously, roughness on multi-length scales was characterized under different magnifications. The 10× objective imaged larger surface features over a sampling area of approximately 1 mm^2, whereas the 50× objective examined a much smaller area and provided structural details on a finer scale. On the larger length scale (Fig. 1B), the surface roughness at the high conversion end (0 mm) generally increased with increased polymer content, with S5 (80% matrix by mass) showing the greatest roughness. In fact, S5 had the roughest surface at all positions along the conversion gradient. The increased roughness on S5 is likely a consequence of the higher polymer content, as it is the polymer itself that exhibits the shrinkage. For all compositions, surface roughness increased as DC decreased until 30 mm, after which some compositions decreased in roughness. Results obtained using the 50× objective (Fig. 1C) showed that the roughness at the high conversion end was comparable for all compositions. Roughness then increased as conversion decreased for all compositions. The different trends in surface roughness between the 10× and 50× objectives indicate that the features are not self-similar across multiple length scales since the RMS roughness values do not scale with size.

The DC, modulus (E), and hardness to modulus ratio (H/E) maps for the composition–conversion gradient are illustrated in Fig. 2. A higher DC was achieved with increased exposure to irradiation (Fig. 2A) for all compositions, in a similar manner as observed for the pure polymer [4]. For the current system, S1 had a slightly lower DC when compared to other compositions ($P < 0.05$), but the deviation was small and primarily occurred at position 0 mm. S2–S5 were statistically identical for any given position along the conversion gradient. These results show that the filler content does not strongly affect the DC for the formulations described within this study. Previous studies have shown that a vitrification effect due to a smaller amount of polymerization exotherm generated in higher filler content samples could result in reduced DCs. However, our results ($n = 10$) showed that vitrification did not play a significant role in this system. Given that the differences between S1 and the other compositions were small, we chose to treat DC as equivalent for all compositions at

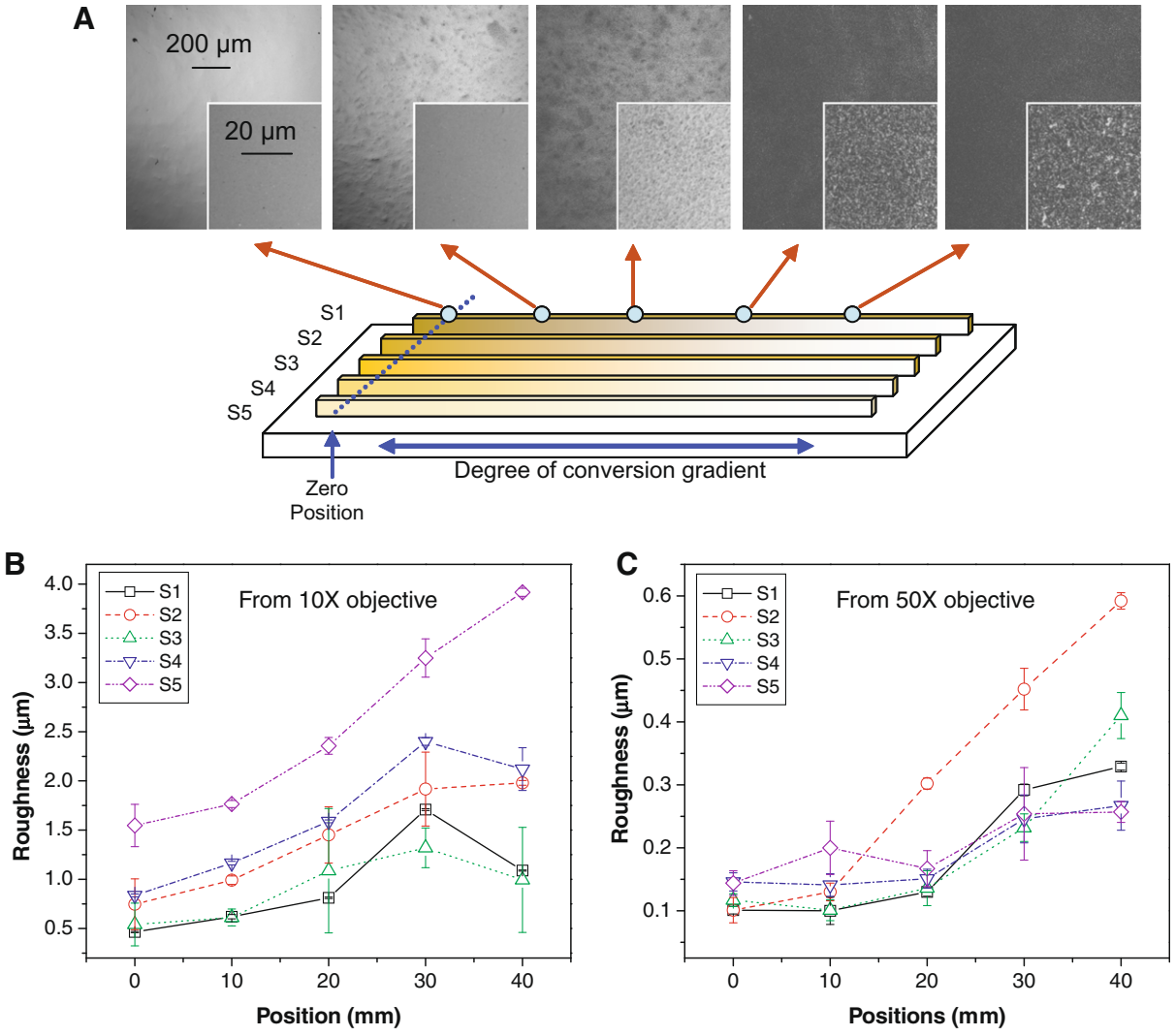

Fig. 1. The gradient samples consisted of five discrete compositions each varying in DC. (A) LSCM (10× objective, and inset 50× objective) was used to image the surface roughness. RMS roughness was calculated for a composite gradient using (B) a 10× objective and (C) a 50× objective. Error bars represent one standard deviation ($n = 3$) and are the estimate of standard uncertainty. Lines are drawn to aid the reader's eyes.

any given position along the DC gradient, and material properties were compared as a function of position from here forward.

The corresponding moduli map (Fig. 2B) for the gradient sample shows a profile similar to the DC map. The modulus of S1 (highest filler loading) was notably higher than that of the other compositions throughout the entire conversion gradient. This trend is observed despite the fact that S1 had a slightly lower DC than the other compositions, indicating the importance of utilizing a high filler loading to increase the elastic modulus. Although S2, S4 and S5 had different filler loading and types, the difference in modulus at the higher DCs, while evident, were more modest among these formulations. (S3 showed an unexpected but reproducible low modulus at high DC. The reasons for this observation are unknown.) The moduli for S2–S5 at low DCs were markedly lower than those observed for S1. Since the filler particles are silanized and can react with the polymerized network, it is possible that a more highly cross-linked network resulted from S1 even at reduced DC, and hence increased the modulus.

Modulus results from nanoindentation were also compared to values obtained using traditional mechanical testing (Fig. 3). Samples with a DC matching that of the 10 mm position on the gradients were prepared and tested using an Instron. The moduli from the two testing methods were comparable for all compositions, validating indentation as a viable tool for producing quantitative mechanical data comparable to traditional testing methods. Several trends in composite modulus were observed as function of filler type and content. First, in comparing S1 and S2, both of which contain only macrofiller, S1 had a higher modulus, due to the overall increase in filler content. S3–S5 contained both nanofiller and macrofiller, and the expected trend of increased modulus with increased filler content was also observed. S2 and S3 contained the same filler content, but S2 contained only macrofiller, whereas S3 contained both nanofiller and macrofiller. S3 exhibited

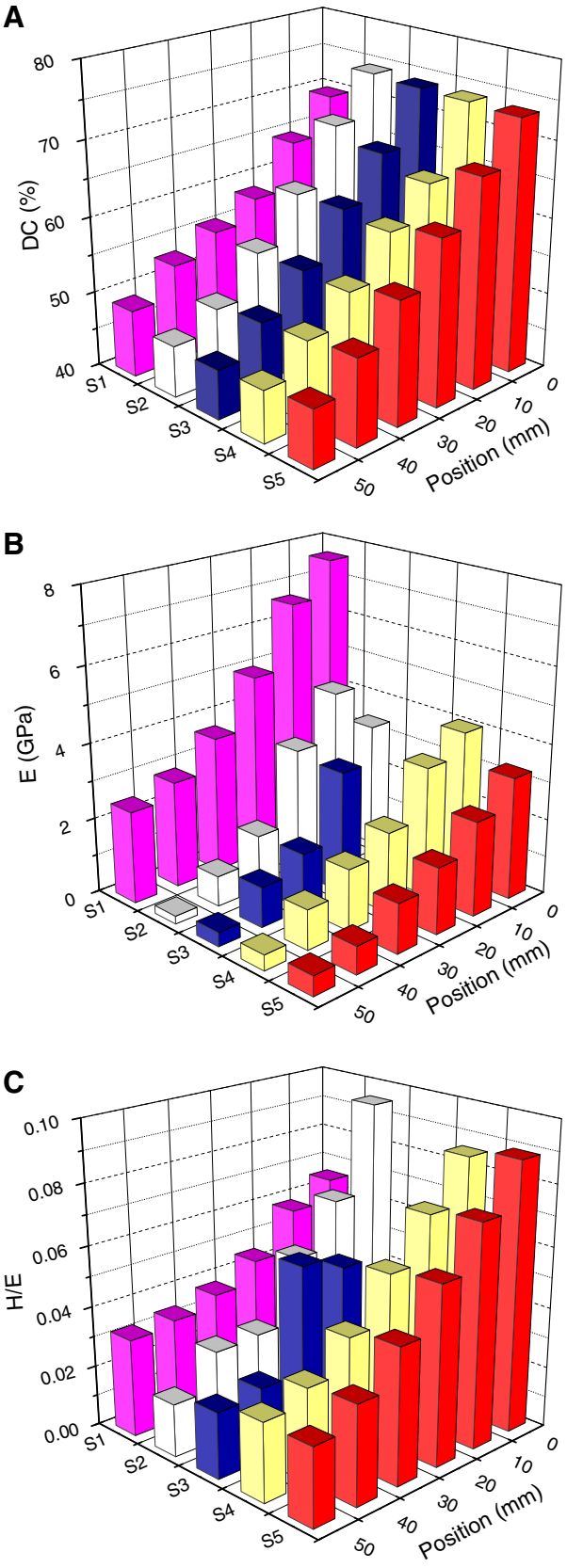

Fig. 2. (A) Degree of conversion, (B) modulus and (C) hardness-to-elastic modulus ratio (H/E) as a function of composition and irradiation (position).

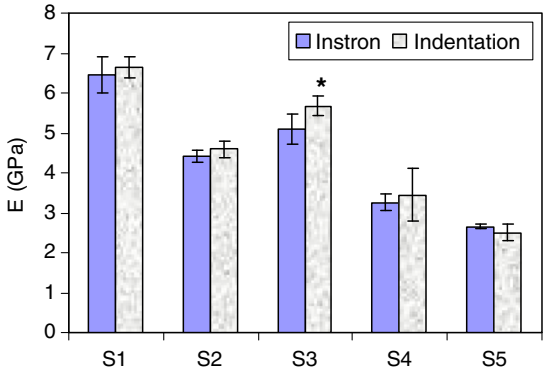

Fig. 3. Moduli obtained by Instron ($n = 5$) and nanoindentation ($n = 3$). The nanoindentation data (except S3) correspond to moduli measured at the 10 mm position, where DC was equivalent to the samples tested by Instron. The nanoindentation modulus for S3 (*) was obtained separately on the fractured samples from the Instron test ($n = 20$). Error bars represent one standard deviation and are the estimate of standard uncertainty.

a slightly higher modulus, probably due to the presence of the nanofiller.

The H/E ratio (Fig. 2C) is a qualitative approach for estimating the scratch performance of materials and coatings, with a higher H/E indicating improved scratch resistance and wear [27]. The highest H/E ratio occurred in the region of highest DC and was due to the increase in hardness, which tends to outpace the increase in modulus as DC increased. For all compositions, an increased H/E ratio was observed as DC increased, indicating that the materials became more resistant to plastic deformation at higher DCs. S2–S5 showed qualitatively similar results at each position, while S1 exhibited less change in the H/E profile. These results suggested that S1 may have different scratch resistance as compared to the other compositions. S2–S5, on the other hand, were expected to show no significant differences in their scratch resistance despite the varied filler content. Specifically, at position 0 mm, the H/E value was higher for S2–S5 than for S1, suggesting that S1 is less scratch resistant at this position, which was unexpected because S1 is the most highly filled composition and has a higher modulus than the other compositions. At lower DCs, the data suggested a transition to a higher scratch resistance for S1 as compared to other compositions. Although some differences were evident with respect to filler size and concentration, the degree of conversion had a dominant effect on the H/E ratios. The scratch resistance estimated here by the H/E ratio will be compared to scratch test results described below.

Progressive load scratch tests were used to characterize the response of the 2-D array sample to scratch damage. The entire scratch profile was examined by confocal microscopy as a function of position (data for S2 are shown in Fig. 4A). All composites exhibited two modes of deformation at high DCs (DC $\geqslant$ 65%), e.g. elastic and plastic. Below a DC of 65%, the scratch resulted in three

modes of deformation with the addition of fracture deformation. Elastic deformation was observed at low scratch loads whereby the composite was able to fully recover after removal of the normal load. A larger scratch load resulted in elastic and plastic deformation, with the plastic deformation manifested as ductile grooving that transitioned into ploughing with increasing applied normal force [28]. The 3-D profiles of the scratches at high load, imaged using confocal microscopy via the 150× objective, showed fractures extending from the walls of the scratch at low DC (Fig. 4B, arrows). In addition, the surface roughness increased with decreasing DC, similar in magnitude to the features observed using the 50× objective. The corresponding depth profiles (Fig. 4C) taken at ~50 mN force show the following trends: (i) the pile-up became less pronounced with decreased DC, due to increased material compliance and increased surface roughness, and (ii) the scratches became wider and deeper with decreased DC, consistent with a more compliant material. A similar trend was observed for all compositions and showed that the compliance increased as DC decreased.

From the depth profiles (Fig. 4C), the scratch deformation was quantified in terms of full depth (D_f), peak-to-peak position (W_p), and their ratio (W_p/D_f). A schematic representation of D_f and W_p is illustrated in Fig. 5A (inset). For all composites, D_f increased as DC decreased (Fig. 5A). At the 0 mm position (highest DC), D_f ranged from 0.4 to 0.6 μm and did not change significantly with filler type and content. Differences in D_f became apparent as DC decreased. At the 10 mm position (DC ≈ 65%), S1 and S5 showed the lowest D_f, whereas S2, S3 and S4 showed a statistically higher D_f. This trend continued qualitatively as DC decreased. The filler concentration was inversely related to W_p at high DC (0 mm position), as the scratches were wider for composites with less filler (Fig. 5B). With the exception of the lowest DC of S1 (40 mm) and the highest DC for S2 (0 mm), W_p increased with decreased DC. We note that it was difficult to determine accurately the peak of the pile-up at low DCs due to an increase in surface roughness. These difficulties may have introduced errors and increased uncertainties in D_f and W_p. W_p/D_f decreased as DC decreased for all compositions (Fig. 5C). For any

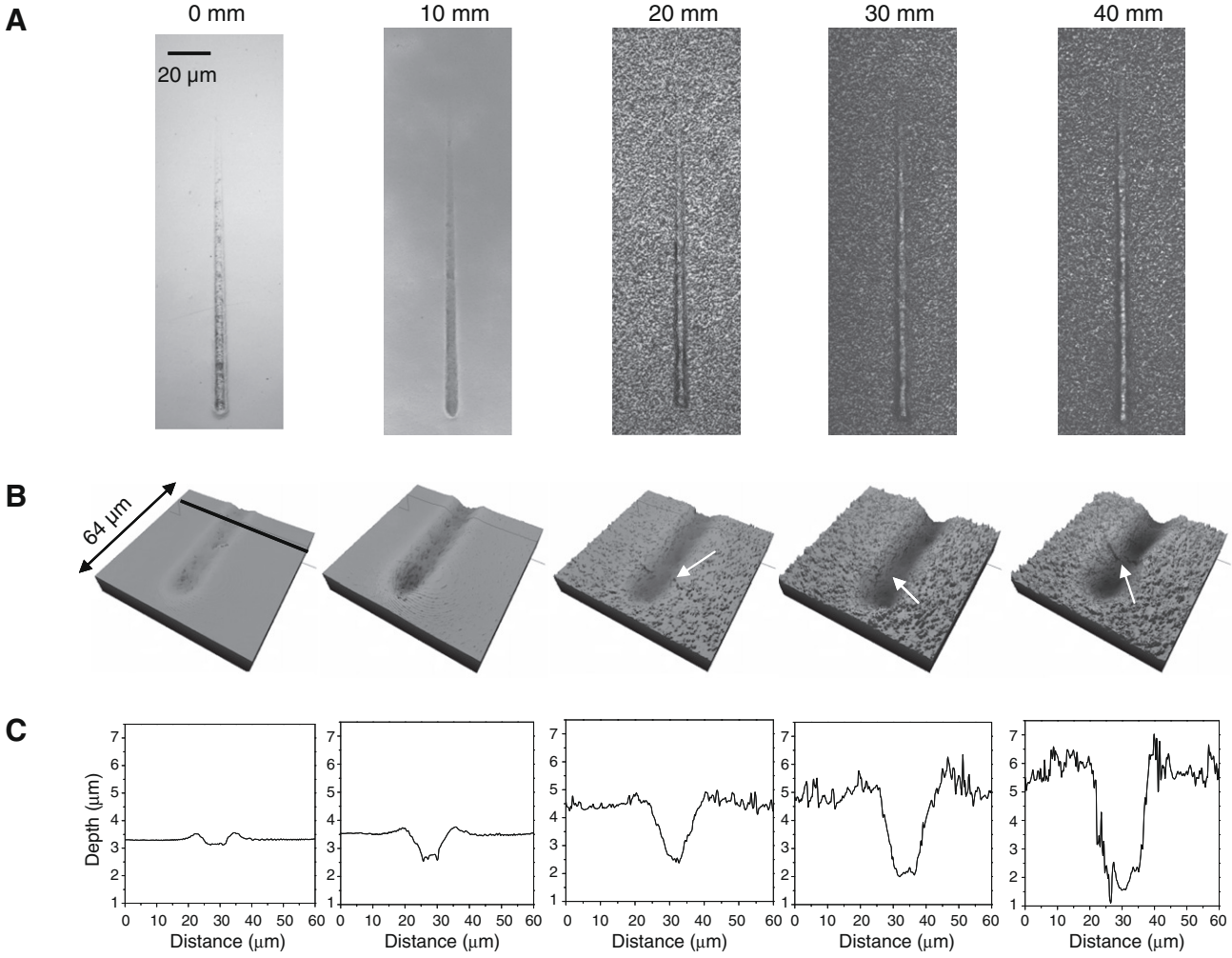

Fig. 4. Progressive load scratches (400 μm in length) measured along the conversion gradient for a single composition (S2). (A) LSCM image of the scratch at each position, (B) 3-D LSCM projection (150× objective) of the 50 mN normal force section of the scratches (arrows indicate fractures), and (C) depth profile of the scratches at approximately 50 mN normal force (black line drawn on the left image in B).

given position, S5 exhibited the highest W_p/D_f. Thus, when width was normalized by depth, the scratches were widest in the least filled S5. These differences were less pronounced for composites with higher filler content. With respect to DC, scratch resistance determined by progressive scratch testing agreed well with that predicted by the H/E ratio in the indentation measurement. In both cases, DC was the dominant variable affecting the scratch deformation, and filler size and concentration did not show a clear effect on the properties.

Another useful analysis method for quantifying the material properties is to compare the initial penetration curves with the residual penetration curves from scratch measurements (Fig. 6A). The initial penetration depth (d_i) is related to the elastic, plastic and viscoelastic (i.e. damage that recovers with time) deformation induced by the inden-

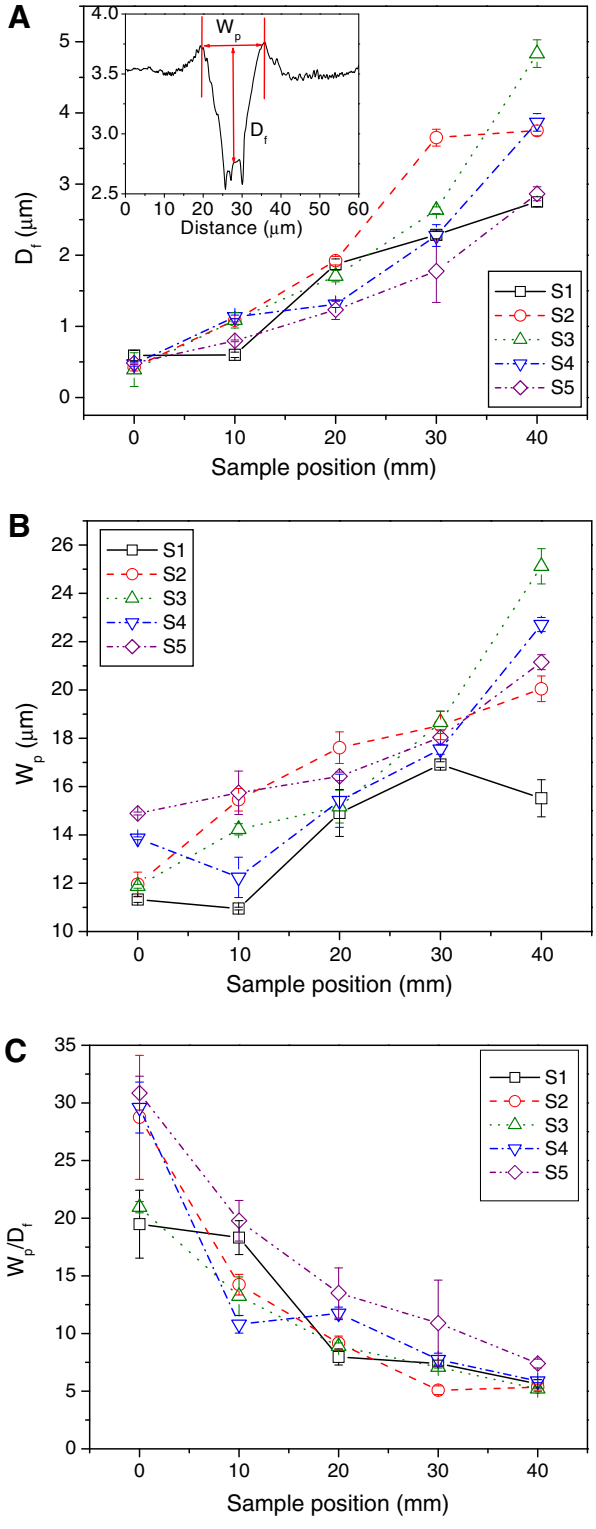

Fig. 5. Scratch parameters (A) D_f, (B) W_p and (C) the ratio of W_p/D_f for various compositions determined along the conversion gradient. The scratch parameters are defined in the inset of (A). Data points are the average value ($n = 3$), and error bars represent one standard deviation and are the estimate of standard uncertainty. Lines are drawn to aid the reader's eyes.

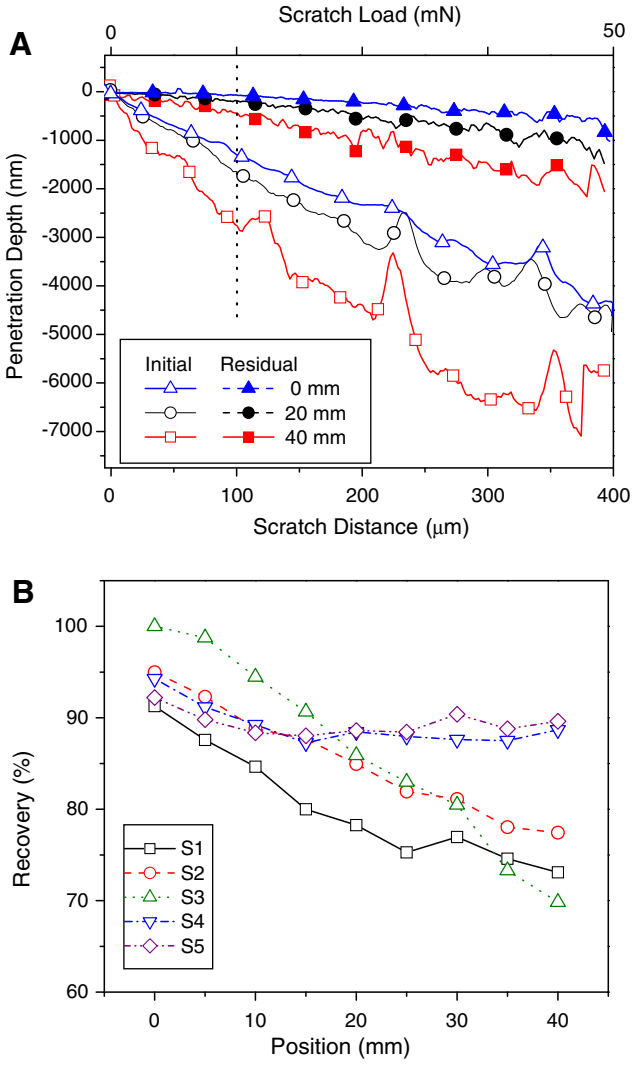

Fig. 6. (A) Initial (open symbols, d_i) and residual (filled symbols, d_r) scratch penetration depths measured as a function of scratch distance and load for S2 at positions of 0, 20 and 40 mm. (B) Scratch recovery determined at a scratch load of 12.5 mN (dashed vertical line in A). The recovery data were the average from three progressive-load scratch tests. Due to varying surface roughness, standard uncertainties range from 3% at higher DC (positions 0–20 mm) to 7% at higher DC (positions greater than 20 mm). Lines are drawn to aid the reader's eyes.

ter tip. The residual penetration depth (d_r) curve reflects residual plastic and any prolonged viscoelastic deformation. Both d_i and d_r curves were relatively smooth at high DCs, indicating primarily ductile grooving of the tip into the sample. As DC decreased, d_i and d_r were deeper, consistent with decreased sample stiffness and hardness. In addition, the penetration profiles, particularly the d_i, became rough (bumpy) indicating potential fracture. Since the samples were composites with potential clusters of fillers, it is also possible that some of the bumps resulted from driving the indenter into stiffer, filler-rich regions.

The difference between d_i and d_r at any given force is the scratch recovery and provides a measure of elastic vs. plastic deformation. A high recovery is indicative of elastic recovery, whereas a lower recovery suggests significant plastic deformation. Fig. 6B plots the percentage recovery determined at a force of 12.5 mN for all compositions and positions. The recovery of scratches at long times was not investigated. Overall, S1 exhibited the lowest recovery, and the recovery diminished with decreased DC. The low recovery observed for S1 is due to the high filler content, as it is the polymer, and not the filler, that provides the recovery. Compared to S1, decreased filler content in S2 shifted the recovery curve slightly upwards, but recovery still decreased with DC. The greatest recovery was observed for S3 at the 0–20 mm positions. Interestingly, although S3 had the highest recovery at high DC, it also had the lowest recovery at low DC. Conversely, the D_f and W_p results for S3 did not exhibit significantly different damage behavior to the other com-

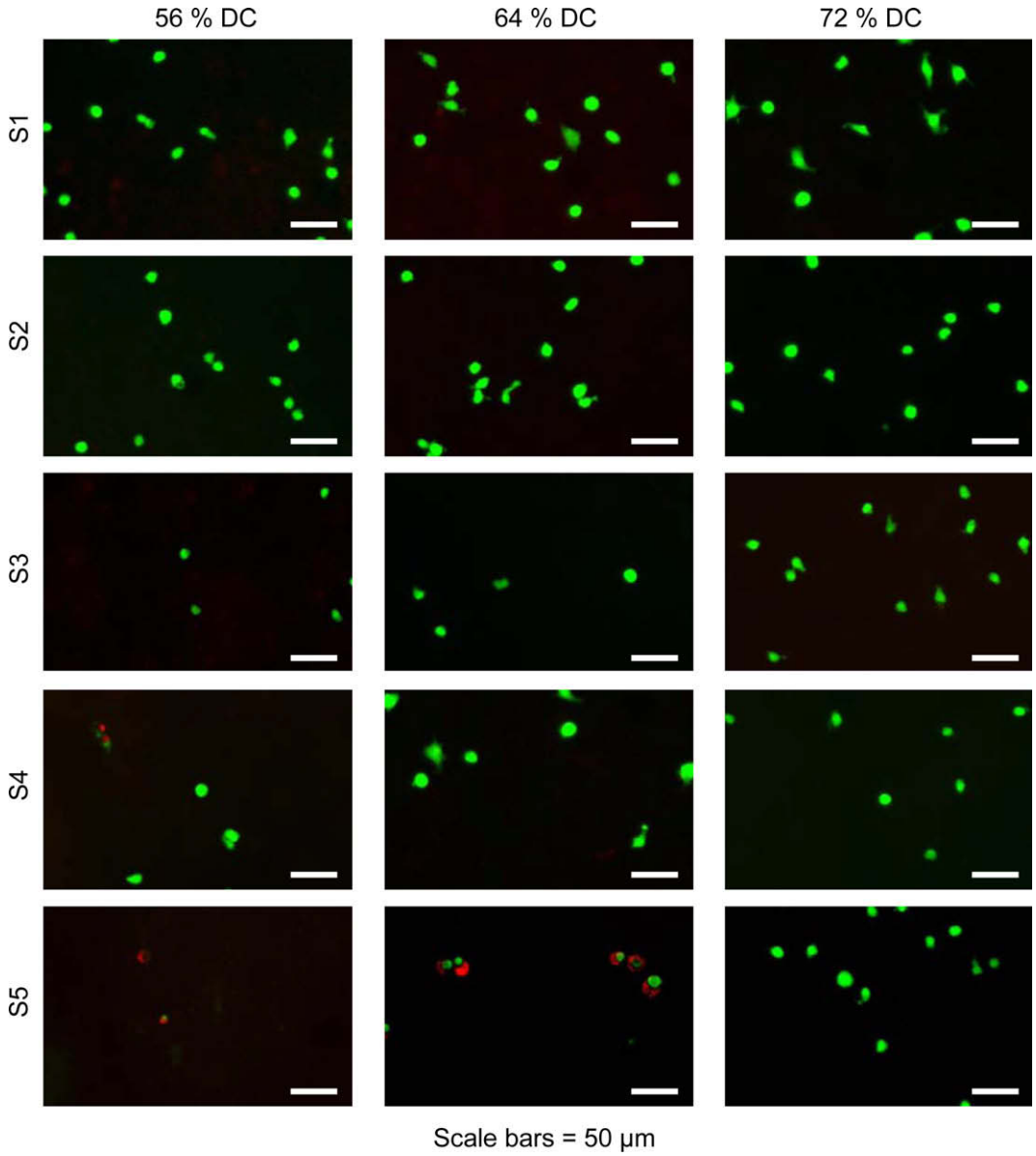

Fig. 7. Macrophage response as a function of composition and DC. Images show cell viability, with green indicating live cells (calcein AM) and red indicating dead cells (EthD-1). Scale bars = 50 μm. (For interpretation of the references to color in this figure legend, the reader is referred to the web version of this paper.)

positions. S2 and S3 had the same total filler mass, but S3 contained nanofiller; therefore, the nanofiller appears to contribute to the modified recovery. It is believed that the addition of nanoparticles may have significantly impacted the viscoelastic behavior of the material near the surface, but this exact behavior is difficult to quantify. While the addition of various filler loadings and sizes minimally affected the modulus and hardness for all compositions, the recovery profiles clearly indicate inherent differences in the viscoelastic responses of these composites. When the total filler proportion was reduced to 35% or less in S4 and S5, no significant reduction in recovery was evident at low DC levels. Both compositions exhibited a relatively flat recovery curve as a function of decreasing DC. This behavior is impressive considering the greater depth and width in the scratch geometry within the low DC region and is probably the result of the large polymer content.

After characterizing the surface mechanics and physical properties using the 2-D platforms, the cell response was also investigated on the same platforms. To evaluate the effects of the surface properties on the biological response, RAW 264.7 macrophages were cultured directly on the 2-D samples. Macrophages are inflammatory cells that are involved in the first line of defense against foreign objects in the body and are therefore useful when evaluating cell–material interactions. The viability stain revealed differences in cell response as a function of composition and DC (Fig. 7). Macrophage viability decreased at low DC only for S4 and S5, the compositions with the lowest filler content [15]. Since the neat polymer has also been shown to be toxic at low DC [14], cell death at lower conversions in S4 and S5 is due to the increased presence of undercured polymer. Cell density also decreased as a function of decreasing DC for S4 and S5 [15].

As discussed earlier, the effects of the nanofiller were evident in the surface morphology, modulus and scratch recovery. The nanofiller also affected the cell behavior on the composites. These effects are best illustrated when comparing S2 and S3, as they both have 50% total filler mass fraction, with S2 containing only macrofiller and S3 containing macrofiller and nanofiller. Neither sample had a significant reduction in cell viability as the DC decreased, which was expected. When evaluating cell density, however, S3 had a significant decrease in cell density at lower conversions, whereas S2 did not (Fig. 7). It is likely that the presence of the nanofiller in S3 contributed to the reduced cell density on S3 at low DC.

Although not all of the assays showed definitive effects with respect to filler type, cell density, surface morphology, mechanical properties and scratch recovery, all indicated a significant role for the presence of the nanofiller. Using combinatorial array samples and a number of measurement techniques, we were able to identify some of the effects of composition and DC on the material properties, even with the complex formulations of photopolymerized composite materials.

4. Conclusions

The 2-D array platform presented in the current study is suitable for quantifying multiple material properties and biological response on the same sample. This study highlights the use of LSCM, DSI and scratch testing in conjunction with gradient substrates to evaluate surface topology and mechanical properties. In addition, cytotoxicity was assessed, and results were compared with the physical and mechanical properties of the substrate. For each substrate, composition was varied discretely by changing the filler content and filler type (with or without nanofiller), and continuous gradients in degree of conversion were fabricating during photopolymerization. Overall, the results suggest that filler mass fraction, the presence of nanofiller and the DC work in concert to affect the surface properties, mechanical properties and the cell response. The combinatorial approach was advantageous for this study, as it provided a more thorough evaluation of the materials and enabled the screening of a number of material parameters.

Acknowledgments

Financial support was provided through an NIDCR/NIST Interagency Agreement Y1-DE-7005-01. The dental resins and fillers were kindly donated by Esstech Inc. and L.D. Caulk Company, respectively.

References

[1] Ferracane JA. Materials in dentistry: principles and application. 2nd ed. Baltimore, MD: Lippincott; 2001.
[2] Amis EJ. Nat Mat 2004;3:83.
[3] Johnson PM, Reynolds TB, Stansbury JW, Bowman CN. Polymer 2005;46:3300.
[4] Lin-Gibson S, Landis FA, Drzal PL. Biomaterials 2006;27:1711.
[5] Barnes SE, Cygan ZT, Yates JK, Beers KL, Amis EJ. Analyst 2006;131:1027.
[6] Simon CG, Eidelman N, Deng Y, Washburn NR. Macromolec Rapid Commun 2004;25:2003.
[7] Tweedie CA, Anderson DG, Langer R, Van Vliet KJ. Adv Mater 2005;17:2599.
[8] Warren OL, Wyrobek TJ. Measure Sci Technol 2005;16:100.
[9] He LH, Swain MV. Dental Mater 2007;23:814.
[10] Drummond JL. J Biomed Mater Res B 2006;78B:27.
[11] Sung LP, Drzal PL, VanLandingHam MR, Wu TY, Chang SH. Jct Res 2005;2:583.
[12] VanLandingHam MR, Sung LP, Chang NK, Wu TY, Chang SH, Jardret VD. Jct Res 2004;1:257.
[13] Lin NJ, Bailey LO, Becker ML, Washburn NR, Henderson LA. Acta Biomater 2007;3:163.
[14] Lin NJ, Drzal PL, Lin-Gibson S. Dental Mater 2007;23:1211.
[15] Lin NJ, Hu.H, Sung LP, Lin-Gibson S. Combinatorial Chemistry; High Throughput Screening, in press.
[16] Bailey LO, Washburn NR, Simon CG, Chan ES, Wang FW. J Biomed Mater Res A 2004;69A:305.
[17] Rakich DR, Wataha JC, Lefebvre CA, Weller RN. J Endodontics 1999;25:114.
[18] Paranjpe A, Bordador LCF, Wang MY, Hume WR, Jewett A. J Dental Res 2005;84:172.
[19] Corle TR, Kino GS. Confocal scanning optical microscopy and related imaging systems. New York: Academic Press; 1996.

[20] Sung LP, Jasmin J, Gu XH, Nguyen T, Martin JW. Jct Res 2004;1:267.
[21] Asif SAS, Wahl KJ, Colton RJ. Rev Sci Instr 1999;70:2408.
[22] VanLandingHam MR. J Res Natl Inst Stand Technol 2003;108:249.
[23] Masouras K, Silikas N, Watts DC. Dental Mater 2008;24:932.
[24] Sung LP, Drzal PL, VanLandingHam MR, forster AM. Metrology for characterizing the scratch resistance of polymeric coatings through optical scattering. Scratching of materials and applications. Amsterdam: Elservier; 2006.
[25] Sun JR, Lin-Gibson S. Dental Mater 2008;24:228.
[26] Kloosterboer JG. Adv Polym Sci 1988;84:1.
[27] Gauthier C, Durier AL, Fond C, Schirrer R. Tribology Int 2006;39:88.
[28] Gauthier C, Lafaye S, Schirrer R. Tribol Int 2001;34:469.